Draft version April 13, 2022
Typeset using LaTeX default style in AASTeX631

Multi-spacecraft analysis of the properties of Magnetohydrodynamic Perturbations in Solar Wind turbulence at 1 au

S. Q. Zhao [1,2] Huirong Yan [1,2] Terry Z. Liu [3] Mingzhe Liu [4] and Huizi Wang [5]

[1] Deutsches Elektronen Synchrotron DESY, Platanenallee 6, 15738, Zeuthen, Germany
[2] Institut für Physik und Astronomie, Universität Potsdam, D-14476, Potsdam, Germany
[3] Department of Earth, Planetary, and Space Sciences, University of California, LA, USA
[4] LESIA, Observatoire de Paris, Université PSL, CNRS, Sorbonne Université, Université de Paris, place Jules Janssen, 92195, Meudon, France
[5] Centre for Shandong Key Laboratory of Optical Astronomy and Solar-Terrestrial Environment, Institute of Space Sciences, Shandong University, Weihai, China

Submitted to APJ

ABSTRACT

We present observations of three-dimensional magnetic power spectra in wavevector space to investigate the anisotropy and scalings of sub-Alfvénic solar wind turbulence in low-β_p plasma at magnetohydrodynamic (MHD) scale using the Magnetospheric Multiscale spacecraft. The magnetic power distributions are organized in a new coordinate determined by wavevectors ($\hat{\mathbf{k}}$) and background magnetic field ($\hat{\mathbf{b_0}}$) in Fourier space. This study utilizes two approaches to determine wavevectors: the singular value decomposition method and multi-spacecraft timing analysis. The combination of both methods allows an examination of magnetic field fluctuation properties in terms of mode compositions without spatiotemporal hypothesis. Observations show that fluctuations ($\delta B_{\perp 1}$) in the direction perpendicular to $\hat{\mathbf{k}}$ and $\hat{\mathbf{b_0}}$ prominently cascade perpendicular to $\hat{\mathbf{b_0}}$, and such anisotropy increases with wavenumbers. The reduced power spectra of $\delta B_{\perp 1}$ follow Goldreich-Sridhar scalings: $\hat{P}(k_\perp) \propto k_\perp^{-\frac{5}{3}}$ and $\hat{P}(k_\parallel) \propto k_\parallel^{-2}$. In contrast, fluctuations within $\hat{k}\hat{b}_0$ plane show isotropic behaviors: perpendicular power distributions are approximately the same as parallel distributions. The reduced power spectra of fluctuations within $\hat{k}\hat{b}_0$ plane follow the scalings: $\hat{P}(k_\perp) \propto k_\perp^{-\frac{3}{2}}$ and $\hat{P}(k_\parallel) \propto k_\parallel^{-\frac{3}{2}}$. Comparing frequency-wavevector spectra with theoretical dispersion relations of MHD modes, we find that $\delta B_{\perp 1}$ are probably associated with Alfvén modes. On the other hand, magnetic field fluctuations within $\hat{k}\hat{b}_0$ plane more likely originate from fast modes in low-β_p plasma based on their isotropic behaviors. The observations of anisotropy and scalings of different magnetic field components are consistent with the predictions of current compressible MHD theory. These results are valuable for further studies of energy compositions of plasma turbulence and their effects on energetic particle transports.

Keywords: Solar wind (1534); Space plasmas (1544); Interplanetary turbulence (830); Interplanetary magnetic fields (824); Heliosphere (710)

1. INTRODUCTION

Plasma turbulence is typically characterized by a broadband spectrum of perturbations, transmitting energy across a wide range of spatial and temporal scales (Bruno & Carbone 2013; Verscharen et al. 2019). Plasma turbulence plays a crucial role in solar corona, solar wind, fusion devices, and interstellar medium (Bruno & Carbone 2013; Yan & Lazarian 2008). The large-scale behaviors of plasma turbulence, which have been successfully described using

Corresponding author: Huirong Yan; Terry Z. Liu
huirong.yan@desy.de; terryliuzixu@ucla.edu

magnetohydrodynamic (MHD) models, are of particular astrophysical interest (Kraichnan 1965; Goldreich & Sridhar 1995). The solar wind is easily accessed for in situ measurements of fields and particles, providing a unique laboratory for studying the physics of turbulent plasma observationally (Tu & Marsch 1995; Verscharen et al. 2019). Spacecraft observations and associated modeling have advanced our understanding of the solar wind in the last decades. However, turbulent properties and the three-dimensional structure of fluctuations remain unclear due to the limited number of sampling points and measurement difficulties. Thus, a study of the three-dimensional energy spectrum of the magnetic field is essential for understanding the dynamics of solar wind turbulence and their effects on energetic particle transports (Yan & Lazarian 2002, 2004).

Solar wind fluctuations are anisotropic due to the presence of the local interplanetary magnetic field, which has been suggested in various studies (Matthaeus et al. 1990; Oughton et al. 2015). Satellite observations and simulations have shown the variance, power, and spectral index anisotropy in magnetic field components parallel and perpendicular to the field (Cho & Lazarian 2009; Oughton et al. 2015). Firstly, solar wind fluctuations perpendicular to the background magnetic field ($\mathbf{B}_0$) are typically more significant than parallel components, consistent with the dominance of incompressible Alfvén modes in the solar wind (Bruno & Carbone 2013). Secondly, turbulence energy predominantly transverses to $\mathbf{B}_0$, based on the spatial correlation functions via single and multiple spacecraft measurements (Matthaeus et al. 1990; He et al. 2011). Thirdly, although solar wind fluctuations are often interpreted as a superposition of fluctuations with quasi-two-dimensional turbulence and a minority slab component, the perpendicular fluctuations are non-axisymmetric with respect to $\mathbf{B}_0$, preferentially, in the direction perpendicular to $\mathbf{B}_0$ and the radial direction (Bruno & Carbone 2013).

Theoretical progress has been achieved to understand the anisotropic behaviors. Goldreich & Sridhar (1995) predicted that a scale-dependent anisotropy is present in incompressible strong MHD turbulence. The energy spectra of perpendicular and parallel components are $E(k_\perp) \propto k_\perp^{-\frac{5}{3}}$ and $E(k_\parallel) \propto k_\parallel^{-2}$, respectively. $k_\perp$ and $k_\parallel$ are wavenumbers perpendicular and parallel to $\mathbf{B}_0$, respectively. The smaller turbulent eddies are more elongated along the local mean magnetic field (Cho & Lazarian 2009; Makwana & Yan 2020). A mechanism called three-wave resonant interaction also seems to be responsible for the anisotropy of magnetic field fluctuations (Shebalin & Montgomery 1983; Cho & Lazarian 2002). Furthermore, according to the compressible MHD theory, plasma turbulence can be decomposed into three eigenmodes (Alfvén, slow, and fast modes) in a stationary, homogeneous, isothermal plasma with a uniform background magnetic field (Makwana & Yan 2020; Zhao et al. 2021). The mode compositions of the turbulence can profoundly affect turbulence anisotropy (Yan & Lazarian 2004). Two-order structure functions show that the cascade of Alfvén and slow modes is anisotropic, preferent in the direction perpendicular to the local magnetic field than in the parallel direction, whereas fast modes tend to show isotropic cascade (Cho & Lazarian 2003; Makwana & Yan 2020). Moreover, both Alfvén and slow modes follow the Goldreich and Sridhar scalings, whereas fast modes follow isotropic scalings in low-β_p plasma (Cho & Lazarian 2003; Makwana & Yan 2020). Direct evidence from solar wind observations for the cascade of each mode is still lacking.

To investigate the anisotropy and scalings of solar wind turbulence with respect to magnetic field at MHD scales at 1 au, we calculate three-dimensional power spectra in wavevector space using the Magnetospheric Multiscale (MMS) spacecraft (Burch et al. 2016). Narita et al. (2010) have tried to obtain three-dimensional energy distributions of magnetic field fluctuations using the wave telescope technique in an ordinary mean-field-aligned system. Compared with previous studies, this study organizes the three-dimensional magnetic power distributions in a new coordinate determined by wavevectors ($\hat{\mathbf{k}}$) and background magnetic field ($\hat{\mathbf{b}}_\mathbf{0}$) in Fourier space. These measurements allow an examination of the anisotropy of magnetic field fluctuations in terms of mode compositions. The organization of this paper is as follows. Section 2 describes datasets, analysis methods, and selection criteria. Section 3 offers observations. In Sections 4 and 5, we discuss and summarize our results.

2. DATA AND METHODOLOGY

2.1. *Data*

The study utilizes the magnetic field data from the fluxgate magnetometer (Russell et al. 2016) and the spectrograms of ion differential energy fluxes from the fast plasma investigation instrument (FPI) (Pollock et al. 2016) onboard MMS. The resolutions of survey-mode magnetic field measured by MMS are 8 samples/s and/or 16 samples/s. To provide sufficient time resolution for the timing analysis, we interpolate the magnetic field to a uniform time resolution of 64 samples/s. Due to FPI limitations in measuring plasma moments in the solar wind, proton parameters from the Operating Missions as a Node on the Internet (OMNI) are used to calculate the proton plasma β_p (defined

as $\beta_p = P_p/P_{mag}$; P_p= proton plasma pressure; P_{mag}= magnetic pressure), proton gyro-frequency f_{ci}, and proton gyro-radius r_{ci}.

2.2. *Analysis method*

The magnetic field observed by four MMS spacecraft consists of the background magnetic field and fluctuating magnetic field, i.e., $\mathbf{B} = \mathbf{B}_0 + \delta\mathbf{B}$. The background magnetic field is obtained by averaging the magnetic field within the defined time window, $\mathbf{B}_0 =< \mathbf{B} >$. We calculate three-dimensional power spectra of magnetic field fluctuations with the following steps.

Firstly, the time series of the fluctuating magnetic field is transformed into Fourier space by the Morlet-wavelet transforms (Grinsted et al. 2004). We obtain wavelet coefficients of three components of the fluctuating magnetic field, i.e., $W_{B_{X,GSE}}(f_{sc}, t)$, $W_{B_{Y,GSE}}(f_{sc}, t)$, and $W_{B_{Z,GSE}}(f_{sc}, t)$ at each time t and spacecraft-frame frequency (f_{sc}), where the subscript GSE represents the geocentric-solar-ecliptic coordinates. We utilize the intervals with twice the length of the studied period to eliminate the edge effect due to finite-length time series and cut off the affected periods.

Secondly, we calculate unit wavevectors $\hat{\mathbf{k}}(f_{sc}, t) = \frac{\mathbf{k}}{|\mathbf{k}|}$ using the singular value decomposition (SVD) of the magnetic spectral matrix (Santolík et al. 2003; Zhao et al. 2021). The SVD technique provides a mathematical method to solve the linearized Gauss's law for magnetism ($\mathbf{k} \cdot \delta\mathbf{B} = 0$) that states a divergence-free constraint of magnetic field vectors. The complex matrices of $\delta\mathbf{B}$ in this study are expressed as the wavelet coefficients. The wavevectors $\hat{\mathbf{k}}$ are calculated by SVD method with 32 s resolution, since we find that the wavevectors of low-frequency fluctuations are relatively stationary with varying time resolution.

Thirdly, since MMS spacecraft relative separations are much smaller than the half-wavelength at MHD scales, the properties and propagations of fluctuations from simultaneous measurements by four MMS spacecraft are approximately similar. The wavevectors and background magnetic field are averaged over four spacecraft: $\mathbf{k} = \frac{1}{4}(\hat{\mathbf{k}}_{M1} + \hat{\mathbf{k}}_{M2} + \hat{\mathbf{k}}_{M3} + \hat{\mathbf{k}}_{M4})$ and $\mathbf{B}_0 = \frac{1}{4}(\mathbf{B}_{0,M1} + \mathbf{B}_{0,M2} + \mathbf{B}_{0,M3} + \mathbf{B}_{0,M4})$, where M1, M2, M3, and M4 denote the four MMS spacecraft. We build a new coordinate in Fourier space using the unit vectors of the wavevectors and background magnetic field ($\hat{\mathbf{k}} = \frac{\mathbf{k}}{|\mathbf{k}|}$ and $\hat{\mathbf{b}}_\mathbf{0} = \frac{\mathbf{B}_0}{|\mathbf{B}_0|}$) at each time t and f_{sc}, where the basis vectors of coordinate axes $\mathbf{e}_{||}$, $\mathbf{e}_{\perp 1}$, and $\mathbf{e}_{\perp 2}$ are in $\hat{\mathbf{b}}_0$, $\hat{\mathbf{k}} \times \hat{\mathbf{b}}_0$, and $\hat{\mathbf{b}}_0 \times (\hat{\mathbf{k}} \times \hat{\mathbf{b}}_\mathbf{0})$ directions, respectively. Then, wavelet coefficients are transformed into the new coordinate: $W_{B_{||}}(t, f_{sc})$, $W_{B_{\perp 1}}(t, f_{sc})$, and $W_{B_{\perp 2}}(t, f_{sc})$.

Fourthly, four MMS spacecraft provide six cross correlations for the magnetic field, i.e., $W_{B_l}^{12} = \langle W_{B_l,M1} W_{B_l,M2}^* \rangle$, $W_{B_l}^{13} = \langle W_{B_l,M1} W_{B_l,M3}^* \rangle$, $W_{B_l}^{14} = \langle W_{B_l,M1} W_{B_l,M4}^* \rangle$, $W_{B_l}^{23} = \langle W_{B_l,M2} W_{B_l,M3}^* \rangle$, $W_{B_l}^{24} = \langle W_{B_l,M2} W_{B_l,M4}^* \rangle$, $W_{B_l}^{34} = \langle W_{B_l,M3} W_{B_l,M4}^* \rangle$ (Grinsted et al. 2004), where the angular brackets denote time averaging over 32 s for each f_{sc}, and the subscript l represents $\mathbf{e}_{||}$, $\mathbf{e}_{\perp 1}$, and $\mathbf{e}_{\perp 2}$, respectively. We calculate wavevectors $k_l(t, f_{sc})$ employing the multi-spacecraft timing analysis based on phase differences between the fluctuating magnetic field (with a time resolution of 64 samples/s) measured by four spacecraft.

Fifthly, wavelet power spectra of the magnetic field averaged over four spacecraft at each time t and f_{sc} in component l are given by

$$P_{B_l}(t, f_{sc}) = \frac{1}{4}(W_{B_l,M1} W_{B_l,M1}^* + W_{B_l,M2} W_{B_l,M2}^* + W_{B_l,M3} W_{B_l,M3}^* + W_{B_l,M4} W_{B_l,M4}^*) \quad (1)$$

Combining $P_{B_l}(t, f_{sc})$ and $k_l(t, f_{sc})$, we obtain frequency-wavenumber power spectra of magnetic field fluctuations $P_{B_l}(k_l, f_{sc})$ in the spacecraft frame.

Finally, the magnetic power spectra are transformed into the rest frame of the solar wind by correcting the Doppler shift. The frequency in the rest frame of the solar wind can be obtained by $f_{rest} = f_{sc} - (\mathbf{k} \cdot \mathbf{V}/2\pi)$. Compared to the solar wind flow, four spacecraft are approximately stationary. Thus, $\mathbf{V}$ is roughly equivalent to the solar wind speed. This study exploits the representation of absolute frequencies: $(f_{rest}, \mathbf{k}_l) = (f_{rest}, \mathbf{k}_l)$ for $f_{rest} > 0$, and $(f_{rest}, \mathbf{k}_l) = (-f_{rest}, -\mathbf{k}_l)$ for $f_{rest} < 0$.

2.3. *selection criteria*

We search for events that satisfy the following criteria: (1) The spectrograms of differential energy fluxes show no evidence of high-energy reflected ions from the terrestrial bow shock, suggesting that fluctuations are in the free solar wind without the effects of the ion foreshock. (2) The magnetic field is devoid of strong gradients, discontinuities, and reversals, guaranteeing that plasma can be considered homogenous. (3) The relative amplitudes of magnetic field fluctuations, defined as $\delta B_{rms}/|\mathbf{B}_0| = \sqrt{\langle |\mathbf{B}(t) - \langle \mathbf{B}(t) \rangle|^2 \rangle}/|\langle \mathbf{B}(t) \rangle|$, are much less than 1. Under such a condition,

the nonlinear term (δB^2) is much less than the linear term ($\mathbf{B}_0 \cdot \delta\mathbf{B}$), and thus fluctuations can roughly be considered as a pure superposition of linear modes. (4) Multi-spacecraft methods are sensitive to scales comparable to spacecraft separations and show limitations on much larger and smaller scales (Horbury et al. 2012). In this study, the spacecraft separations are roughly as large as the ion gyro-radius. Therefore, given the applicability of MHD theory and measurement limitation, we only analyze fluctuations within $2/t^* < f_{rest} < f_{ci}$ and $0.01 < kr_{ci} < 0.1$, and set the magnetic power to zero out of this range. The parameter t^* is the duration studied.

The only other criterion used is the requirement that the angle $\phi_{\hat{k}k_l}$ between $\hat{\mathbf{k}}$ (obtained by SVD method) and $\mathbf{k_l}$ (obtained by timing analysis) should be small. Typically, when analyzing solar wind data via single spacecraft, we assume $f_{sc} \propto k$ based on Taylor's hypothesis (Taylor 1938) for a given wave propagation angle θ_{kB_0}. This approximation is considered reliable mainly because the velocity of the solar wind flow (V_{sw}) is much larger than phase speeds of MHD waves. However, the approximation does not always hold even though V_{sw} is much faster than the phase speed of fluctuations, e.g., when fluctuations with wavevectors at large angles from the solar wind flow. Therefore, this study utilizes two methods for accuracy to identify the propagation directions, i.e., the SVD method and multi-spacecraft timing analysis (described in Section 2.2). The latter method allows determining wavevectors independent of any spatiotemporal hypothesis. Our results show that data counts are primarily concentrated in $\phi_{\hat{k}k_l} < 30°$, whereas a small number of counts still exist in large-$\phi_{\hat{k}k_l}$ range. It indicates that not all fluctuations are aligned with the direction of minimum variance vectors of magnetic field fluctuations and satisfy $f_{sc} \propto k$ hypothesis (because the fluctuations are combinations of multiple modes with different dispersion relations). Therefore, we filter out fluctuations with a large $\phi_{\hat{k}k_l}$, which invalidates the SVD assumption. This part of fluctuations is beyond the scope of the present paper and will be the topic of a separate publication. Considering that the fluctuating magnetic field ($\delta B_{\perp 1}$) out of $\hat{k}\hat{b}_0$ plane dominates magnetic power ($\sim 80\%$), the propagation direction of $\delta B_{\perp 1}$ should be mainly aligned with $\hat{\mathbf{k}}$, whereas fluctuations within $\hat{k}\hat{b}_0$ plane accounting for a tiny proportion have little impact on the direction of $\hat{\mathbf{k}}$. Therefore, this study sets a more stringent criterion $\phi_{\hat{k}k_l} < 10°$ for $\delta B_{\perp 1}$ fluctuations and a moderate criterion $\phi_{\hat{k}k_l} < 30°$ for fluctuations within $\hat{k}\hat{b}_0$ plane.

This study presents three representative events in low-β_p solar wind, and their properties are listed in Table 1. These three events are also included in the appendix by Roberts et al. (2020). During these intervals, four spacecraft have a 1-minute time shift from the nose of the terrestrial bow shock, suggesting approximately the same plasma environment observed by MMS and OMNI. Meanwhile, the qualities of MMS tetrahedral configuration are around 0.9, allowing for distinguishing spatial and temporal evolutions and investigating three-dimensional structures of fluctuations.

3. OBSERVATIONS

An overview of three representative events of solar wind fluctuations is shown in Figure 1. For all three events, the magnetic field and plasma parameters are stationary. Figures 1c, 1i, and 1o show the relative amplitudes of the magnetic field $\delta B_{rms}/|\mathbf{B}_0| = \sqrt{\langle|\mathbf{B}(t) - \langle\mathbf{B}(t)\rangle|^2\rangle}/|\langle\mathbf{B}(t)\rangle|$, where the angular brackets denote a time average over 10, 20, and 30 minutes, respectively. $\delta B_{rms}/|\mathbf{B}_0|$ are much less than 1, indicating that the nonlinear term (δB^2) is much less than the linear term ($\mathbf{B}_0 \cdot \delta\mathbf{B}$). Thus, it is valid that fluctuations are considered as a pure superposition of linear MHD modes. Figure 2 shows MMS locations and the directions of the background magnetic field in GSE coordinates for Event 1, Event 2, and Event 3, respectively. As shown in Figure 2, theoretically, the mean magnetic field is either not connected to terrestrial bow shock or nearly tangential to it. Indeed, the spectrograms of ion differential energy fluxes show no evidence of high-energy reflected ions (Figures 1d, 1j, and 1p). Thus, these intervals are free from ion foreshock contaminations. Figures 1e, 1k, and 1q show that three events are in low-β_p solar wind, where proton plasma β_p is calculated by OMNI proton parameters and MMS magnetic field. In Figures 1f, 1l, and 1r, wave propagation angles with respect to the background magnetic field $\langle\mathbf{B}(t)\rangle_{30min}$ (average over 30 minutes) cover 0° to 90°, allowing us to calculate the magnetic power distribution in wavevector space more reliable.

The solar wind fluctuations are closely related to the local background magnetic field. This study explores the variation of the magnetic power distributions with the background magnetic field by adjusting the length of time windows. We split the time intervals of these three events into several moving time windows with a step size of 5 minutes and a length of 10, 20, and 30 minutes, respectively. This study refers to them as 10-minute, 20-minute, and 30-minute datasets. We calculate the background magnetic field ($\mathbf{B}_0$) by averaging the magnetic field in each time window. In this way, $\mathbf{B}_0$ in each time window is constant in time and along the same direction in both real and Fourier space, suggesting that the new coordinate determined by $\mathbf{B}_0$ is independent of the space transformation.

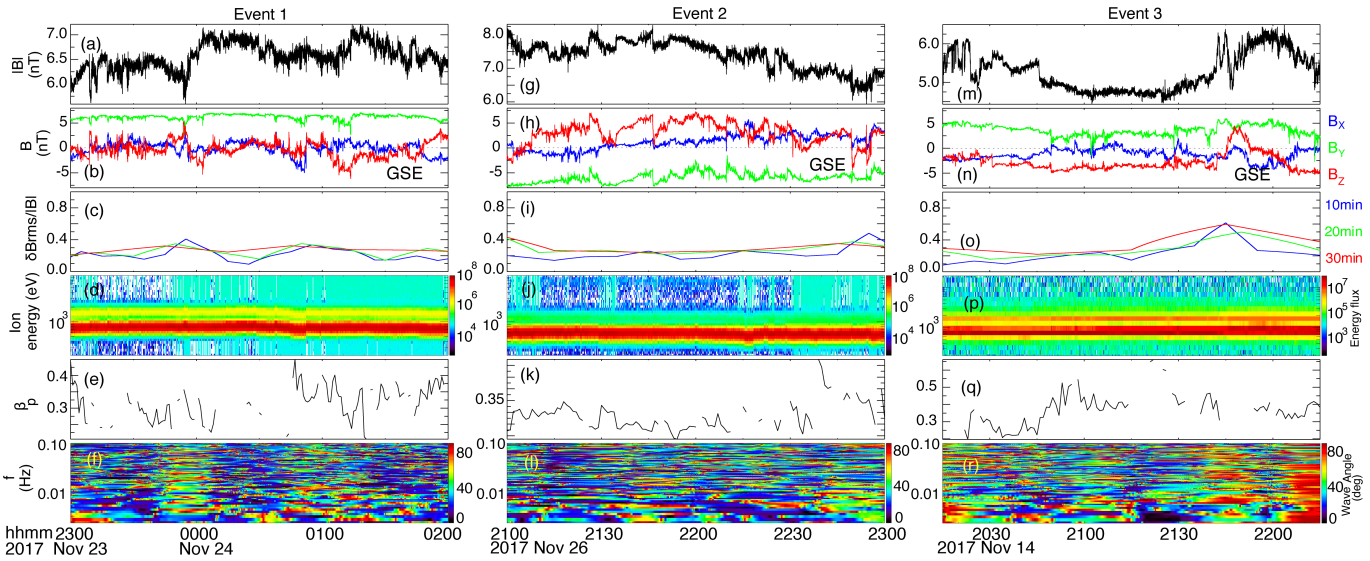

Figure 1. An overview of solar wind fluctuations from MMS1 and OMNI. (a-f) Event 1: during 23:00-02:00 UT on 2017 November 23-24. (g-l) Event 2: during 21:00-23:00 UT on 2017 November 26. (m-r) Event 3: during 20:15-22:15 UT 2017 November 14. The panels from top to bottom show the magnetic field magnitude $|\mathbf{B}|$, magnetic field components in GSE, relative amplitudes of the magnetic field $\delta B_{rms}/|\mathbf{B}_0|$, the spectrogram of ion differential energy fluxes ($keVcm^{-2}s^{-1}sr^{-1}keV^{-1}$), proton plasma β_p, wave propagation angles with respect to the background magnetic field.

To investigate the reliability of employing observational three-dimensional power distributions to describe the structure of solar wind turbulence, we calculate the normalized two-point correlation function $R(\tau)/R(0)$, where $R(\tau)$ is defined as $\langle \delta B(t)\delta B(t+\tau)\rangle$, and τ is the timescale. The results of the three events are similar, and we take Event 1 as an example. Figure 3 shows the normalized two-point correlation function of datasets with a window length of 10, 20, and 30 minutes, respectively. Different time windows (black curves) with a step size of 5 minutes present a similar profile of $R(\tau)/R(0)$, indicating that the correlation function is independent of the starting time; thus, fluctuations are in a homogeneous plasma. Moreover, when well-behaved turbulence becomes uncorrelated ($R(\tau)/R(0) \to 0$), the average values of τ are around 160 s, 280 s, and 370 s, respectively. Therefore, the measured correlation time T_c, estimated by $T_c = \int_0^{R(\tau)\to 0} R(\tau)/R(0)d\tau$ is much less than the window length. As a result, it is reliable to assume that turbulent magnetic field fluctuations are stationary and homogeneous (Matthaeus & Goldstein 1982).

We perform the approaches described in Section 2.2 to calculate three-dimensional frequency-wavenumber magnetic power spectra in the spacecraft frame. Then we transform the magnetic power spectra into the rest frame of the solar wind by correcting the Doppler shift. To obtain $k_\perp - k_{||}$ wavelet power spectra of magnetic field fluctuations, we construct a set of 100×100 bins, where $k_{||}$ represents wavenumber parallel to the background magnetic field ($\mathbf{B}_0$), and $k_\perp = \sqrt{(k_{\perp 1}^2 + k_{\perp 2}^2)}$ represents wavenumber perpendicular to $\mathbf{B}_0$. Each bin subtends approximately the same perpendicular and parallel wavenumber. We sum all magnetic power in each bin at all frequencies and times. To cover all MHD-scale wavenumbers, we set the maximum wavenumber as $k_{max} = k_{\perp,max} = k_{||,max} = 1.1 \times \frac{0.1}{r_{ci}}$, and the step length of each bin is $dk = k_{max}/100$.

3.1. *The results of $\delta B_{\perp 1}$ fluctuations*

Figure 4 shows $k_\perp - k_{||}$ wavelet power spectra of magnetic field fluctuations ($\delta B_{\perp 1}$) out of $\hat{k}\hat{b}_0$ plane using datasets with a length of 10, 20, and 30 minutes, respectively. The magnetic power spectra $\hat{P}_{B_{\perp 1}}(k_\perp, k_{||}) = P_{B_{\perp 1}}(k_\perp, k_{||})/P_{B_{\perp 1,max}}$ are normalized by the maximum power in all bins. From top to bottom, Figures 4a-4c, 4d-4f, and 4g-4i display magnetic power spectra of Event 1, Event 2, and Event 3, respectively. For all events, magnetic power distributions prominently elongate perpendicular to the background magnetic field, indicating a faster cascade in the perpendicular direction. Moreover, we observe an apparent scale-dependent anisotropy: magnetic power spectra

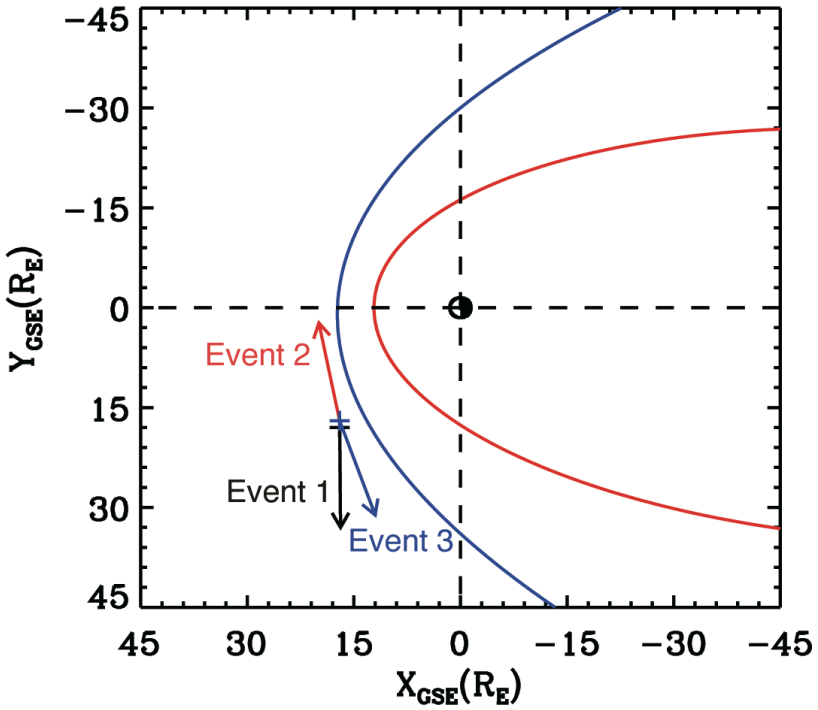

Figure 2. A schematic of MMS locations in GSE coordinates. Blue and red solid curves represent the empirical models of terrestrial bow shock (Peredo et al. 1995) and magnetopause (Roelof & Sibeck 1993). The black, red, and blue arrows represent the directions of the background magnetic field for Event 1 ($[17, 18, 6]R_E$), Event 2 ($[17, 17, 6]R_E$), and Event 3 ($[17, 17, 6]R_E$), respectively.

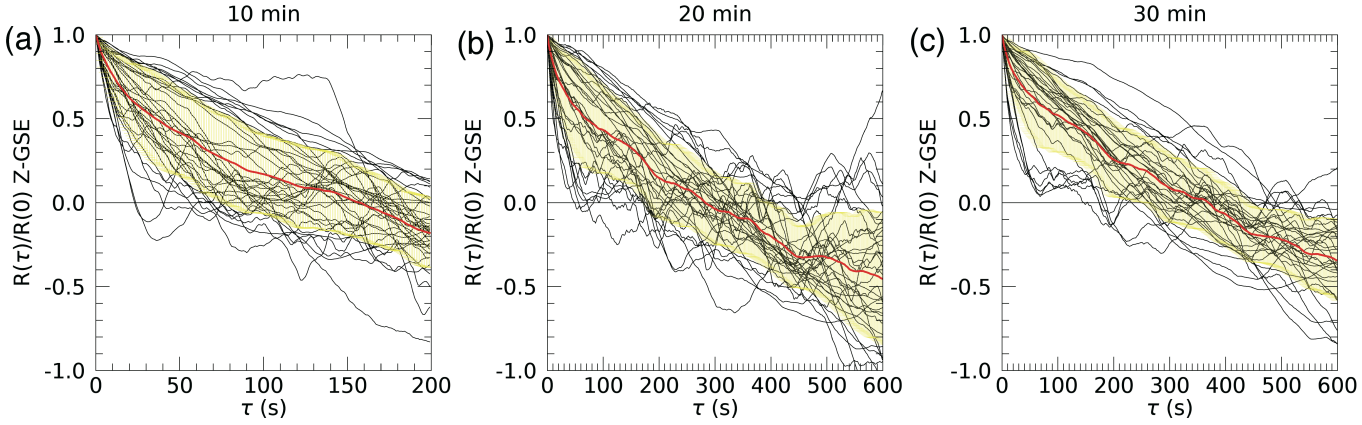

Figure 3. Normalized correlation function $R(\tau)/R(0)$ vs. timescale τ for magnetic field Z_{GSE}-component with a window length of 10, 20, and 30 minutes, respectively, using Event 1 datasets measured by MMS1. The black curves represent the normalized correlation function of each window. The red curves and yellow shaded regions represent average $R(\tau)/R(0)$ and standard errors over all windows, respectively. The horizontal solid lines mark $R(\tau)/R(0) = 0$.

are more stretched along the background magnetic field as the wavenumber increases. Besides, magnetic power spectra show more isotropic behaviors as the window length increases.

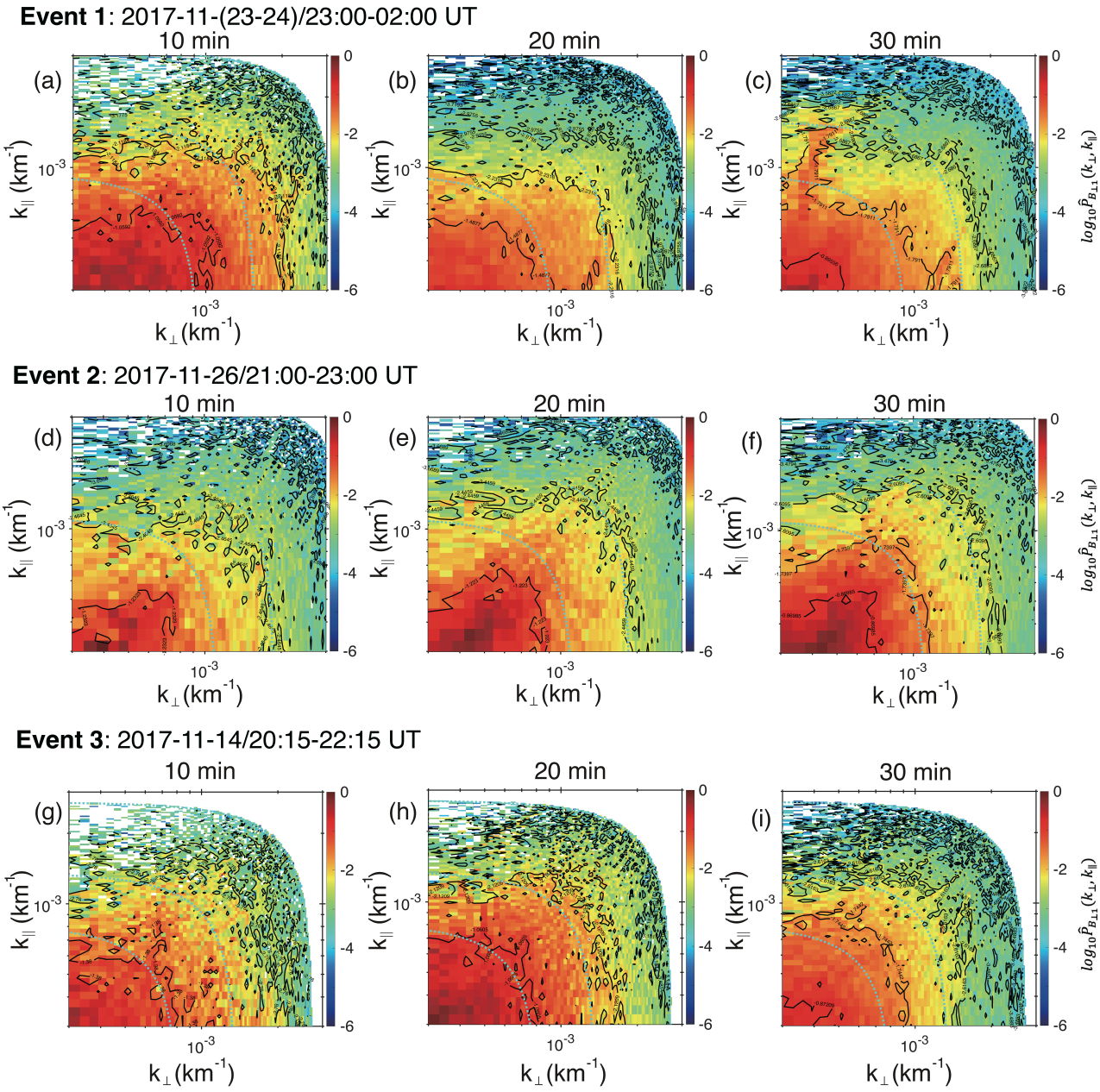

Figure 4. $k_\perp - k_{||}$ wavelet power spectra of magnetic field fluctuations ($\delta B_{\perp 1}$ out of $\hat{k}\hat{b}_0$ plane using datasets with a length of 10, 20, and 30 minutes, respectively. The magnetic power spectra $\hat{P}_{B_{\perp 1}}(k_\perp, k_{||}) = P_{B_{\perp 1}}(k_\perp, k_{||})/P_{B_{\perp 1,max}}$ are normalized by the maximum power in all bins. (a-c) Event 1: during 23:00-02:00 UT on 2017 November 23-24. (d-f) Event 2: during 21:00-23:00 UT on 2017 November 26. (g-i) Event 3: during 20:15-22:15 UT 2017 November 14. The blue dashed curves mark $k = \sqrt{k_{||}^2 + k_\perp^2} = 0.03/r_{ci}$, $0.05/r_{ci}$, and $0.1/r_{ci}$, respectively.

To quantitively analyze these properties of magnetic power spectra, we obtain the one-dimensional reduced magnetic power spectra of $\delta B_{\perp 1}$ by

$$\hat{P}_{B_{\perp 1}}(k_\perp) = \int_0^\infty \hat{P}_{B_{\perp 1}}(k_\perp, k_{||}) dk_{||} \sim \int_{k_{||,min}}^{k_{max}} \hat{P}_{B_{\perp 1}}(k_\perp, k_{||}) dk_{||} \tag{2}$$

$$\hat{P}_{B_{\perp 1}}(k_{||}) = \int_0^\infty \hat{P}_{B_{\perp 1}}(k_\perp, k_{||}) dk_\perp \sim \int_{k_{\perp,min}}^{k_{max}} \hat{P}_{B_{\perp 1}}(k_\perp, k_{||}) dk_\perp \tag{3}$$

The parallel wavenumber can be expressed as $k_{||} \propto k_{\perp}^{\frac{2}{3}}/l_0^{\frac{1}{3}}$, where l_0 is the injection scale (approximately equivalent to the correlation length in this study) (Yan & Lazarian 2008). Here, take Event 1 as an example to estimate the minimum wavenumbers. Given $\delta V/V_A$ can be roughly expressed as $\delta B/B_0$ for incompressible fluctuations, velocity fluctuations δV are around 15 km/s, where Alfvén velocity $V_A \sim 50$ km/s and $\delta B/B_0 \sim \langle \delta B_{rms}/|\mathbf{B}| \rangle_{30min} \sim 0.3$. The correlation time T_c stabilizes at around 400 s, even though using longer time windows (larger than 30 minutes). Thus, the correlation length is around 6000 km. If we assume the minimum perpendicular wavenumber $k_{\perp,min} \sim \frac{0.01}{r_{ci}} \sim 3 \times 10^{-4}$ $km^{-1}(r_{ci} \sim 31.8\ km)$, the minimum parallel wavenumber is $k_{||,min} \sim 2.5 \times 10^{-4}\ km^{-1} \sim k_{\perp,min}$. The calculations can be confirmed by the relationship between $k_\perp$ and $k_{||}$ at the small wavenumbers in Figure 10d.

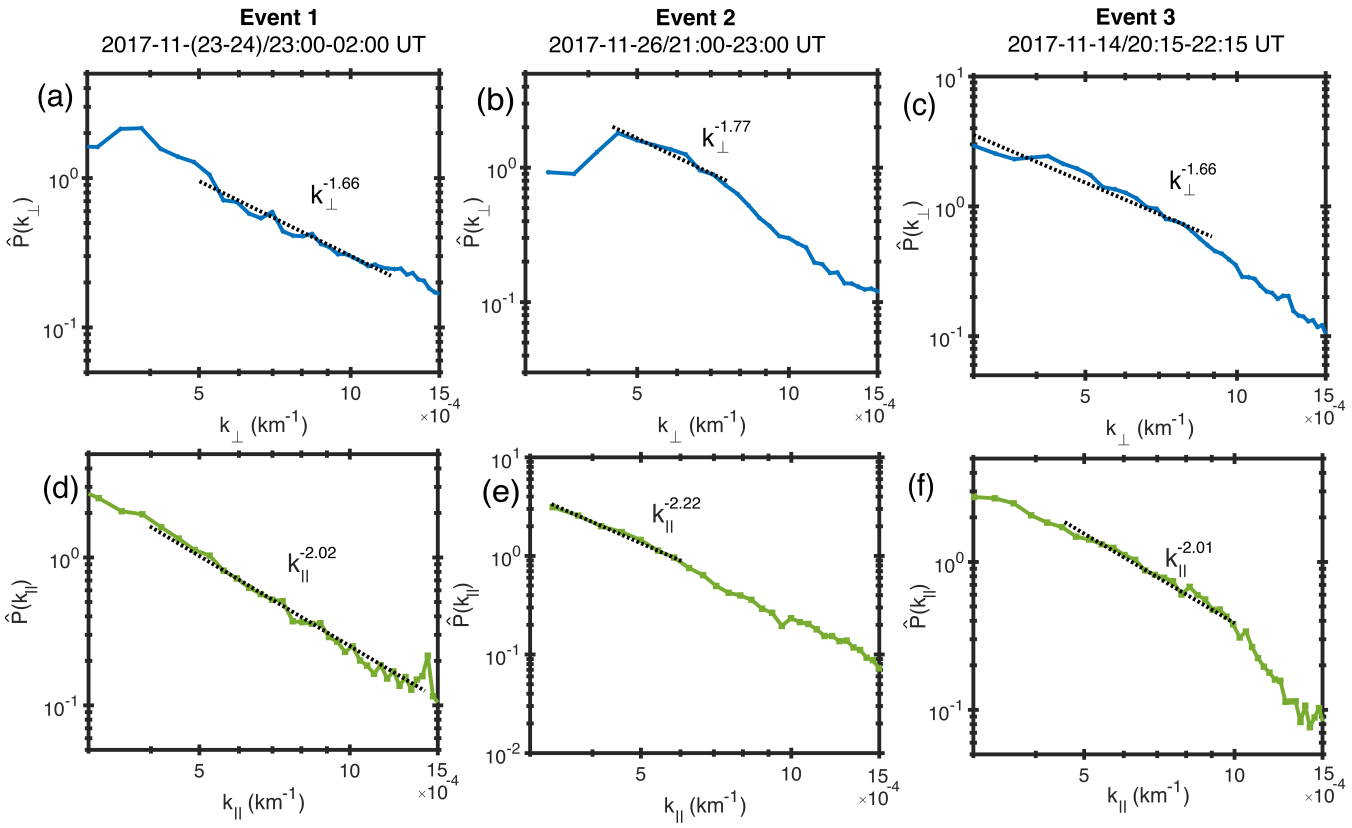

Figure 5. The reduced power spectra of $\delta B_{\perp 1}$ fluctuations using 30-minute datasets. Blue curve $\hat{P}(k_\perp)$: normalized perpendicular wavenumber spectrum of $\delta B_{\perp 1}$ fluctuations; green curve $\hat{P}(k_{||})$: normalized parallel wavenumber spectrum of $\delta B_{\perp 1}$ fluctuations; black dashed line: power-law fits. (a, d) Event 1: during 23:00-02:00 UT on 2017 November 23-24. (b, e) Event 2: during 21:00-23:00 UT on 2017 November 26. (c, f) Event 3: during 20:15-22:15 UT 2017 November 14.

It is challenging to quantitively present magnetic power distributions in wavevector space through limited measurements. However, the longer interval we choose, the observed power spectra are closer to actual distributions. Thus, we present reduced power spectra of $\delta B_{\perp 1}$ fluctuations using 30-minute datasets, although shorter datasets show similar behaviors. Figures 5a-5c show that the normalized perpendicular wavenumber spectra of $\delta B_{\perp 1}$ fluctuations roughly follow a Kolmogorov spectrum: $\hat{P}(k_\perp) \propto k_\perp^{-\frac{5}{3}}$. Figures 5d-5f show that the normalized parallel wavenumber spectra of $\delta B_{\perp 1}$ fluctuations roughly follow $\hat{P}(k_{||}) \propto k_{||}^{-2}$. These scalings are consistent with the Goldreich & Sridhar (1995) theory. For event 1 (3 hours measurements), magnetic power distributions almost follow the Goldreich & Sridhar (1995) scalings from $k_{||} \sim [4 \times 10^{-4}, 1.5 \times 10^{-3}]\ km^{-1}$ (corresponding wavenumber relations are shown in Figure 10d). However, for Events 2 and 3 (2 hours measurements), magnetic power distributions satisfy the scale-dependence scaling only at partial wavenumbers. Besides, their power-law fits are easily affected by the wavenumber ranges, likely because of the incomplete results from the limited-time series.

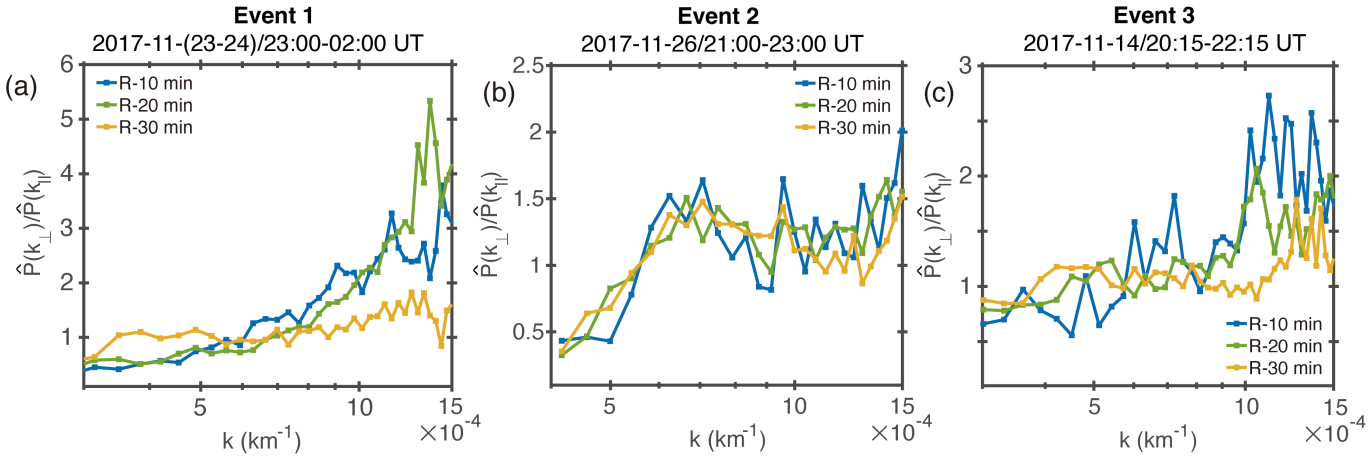

Figure 6. The ratio $\hat{P}(k_\perp)$ to $\hat{P}(k_{||})$ of $\delta B_{\perp 1}$ fluctuations. $\hat{P}(k_\perp)$ represents the normalized perpendicular wavenumber spectrum of $\delta B_{\perp 1}$, and $\hat{P}(k_{||})$ represents the normalized parallel wavenumber spectrum of $\delta B_{\perp 1}$. (a) Event 1: during 23:00-02:00 UT on 2017 November 23-24. (b) Event 2: during 21:00-23:00 UT on 2017 November 26. (c) Event 3: during 20:15-22:15 UT 2017 November 14.

To investigate the anisotropy of magnetic power spectra of $\delta B_{\perp 1}$ fluctuations, we show the ratio $\hat{P}(k_\perp)$ to $\hat{P}(k_{||})$ in Figure 6. Firstly, the ratios $\hat{P}(k_\perp)$ to $\hat{P}(k_{||})$ are much larger than 1 at most wavenumbers, indicating that magnetic field distributions are stretched along the background magnetic field. Secondly, almost all datasets show a similar tendency that the ratio $\hat{P}(k_\perp)$ to $\hat{P}(k_{||})$ increases with the wavenumbers, especially for $k > 5 \times 10^{-4}\ km^{-1}$, suggesting that the anisotropy of magnetic power spectra increases with the wavenumbers. This result is consistent with simulation results: the smaller eddies are more stretched along the background magnetic field (Makwana & Yan 2020). Thirdly, the ratios $\hat{P}(k_\perp)$ to $\hat{P}(k_{||})$ obtained by 10-minute (blue) and 20-minute (green) datasets are larger than those obtained by 30-minute datasets (yellow) at most wavenumbers, especially for $k > 5 \times 10^{-4}\ km^{-1}$. It means that the anisotropy decreases when we use the longer time windows to calculate the background magnetic field. Therefore, these observations provide evidence that solar wind fluctuations are more likely aligned with the local magnetic field based on the size of the fluctuations rather than a global magnetic field.

3.2. *The results of fluctuations within $\hat{k}\hat{b}_0$ plane*

The magnetic field fluctuations within $\hat{k}\hat{b}_0$ plane are composed by $\delta B_{||}$ and $\delta B_{\perp 2}$ components, where $\delta B_{||}$ represents magnetic field fluctuations parallel to B_0, and $\delta B_{\perp 2}$ represents fluctuations perpendicular to B_0 and within $\hat{k}\hat{b}_0$ plane. Based on the ideal MHD theory, this part of magnetic field fluctuations is provided by compressible magnetosonic modes. Figure 7 presents the sum of $k_\perp - k_{||}$ wavelet power spectra of $\delta B_{||}$ and $\delta B_{\perp 2}$ fluctuations, which are normalized by the maximum power in all bins ($\hat{P}_{B_{in\hat{k}\hat{b}plane}}(k_\perp, k_{||}) = (P_{B_{||}}(k_\perp, k_{||}) + P_{B_{\perp 2}}(k_\perp, k_{||}))/(P_{B_{||}} + P_{B_{\perp 2}})_{max}$). Since these sub-Alfvénic fluctuations within $\hat{k}\hat{b}_0$ plane only occupy a tiny part of total magnetic power ($\sim 20\%$), magnetic power cannot cover all wavenumbers. Thus, many vacant bins are present in Figure 7. Nevertheless, magnetic power spectra within $\hat{k}\hat{b}_0$ plane still show explicit isotropic behaviors: the perpendicular magnetic power distributions are comparable to those in the parallel direction.

We calculate one-dimensional reduced power spectra of magnetic field fluctuations within $\hat{k}\hat{b}_0$ plane by Equations (2) and (3) for in-plane components using 30-minute datasets. Although the reliability of quantitative analysis is questionable, the normalized perpendicular wavenumber spectra $\hat{P}(k_\perp)$ are roughly comparable to the parallel wavenumber spectra $\hat{P}(k_{||})$) (Figure 8), and the ratios $\hat{P}(k_\perp)$ to $\hat{P}(k_{||})$ are around 1 (Figure 9). Therefore, the isotropic behaviors are independent of the wavenumbers. Moreover, the reduced power spectra follow a similar scaling $\hat{P}(k_\perp) \propto k_\perp^{-\frac{3}{2}}$ and $\hat{P}(k_{||}) \propto k_{||}^{-\frac{3}{2}}$ in Figure 8. The isotropic scalings are consistent with fast-mode scalings in low-β_p plasma (Cho & Lazarian 2003; Makwana & Yan 2020).

4. FURTHER ANALYSIS ON MHD MODES

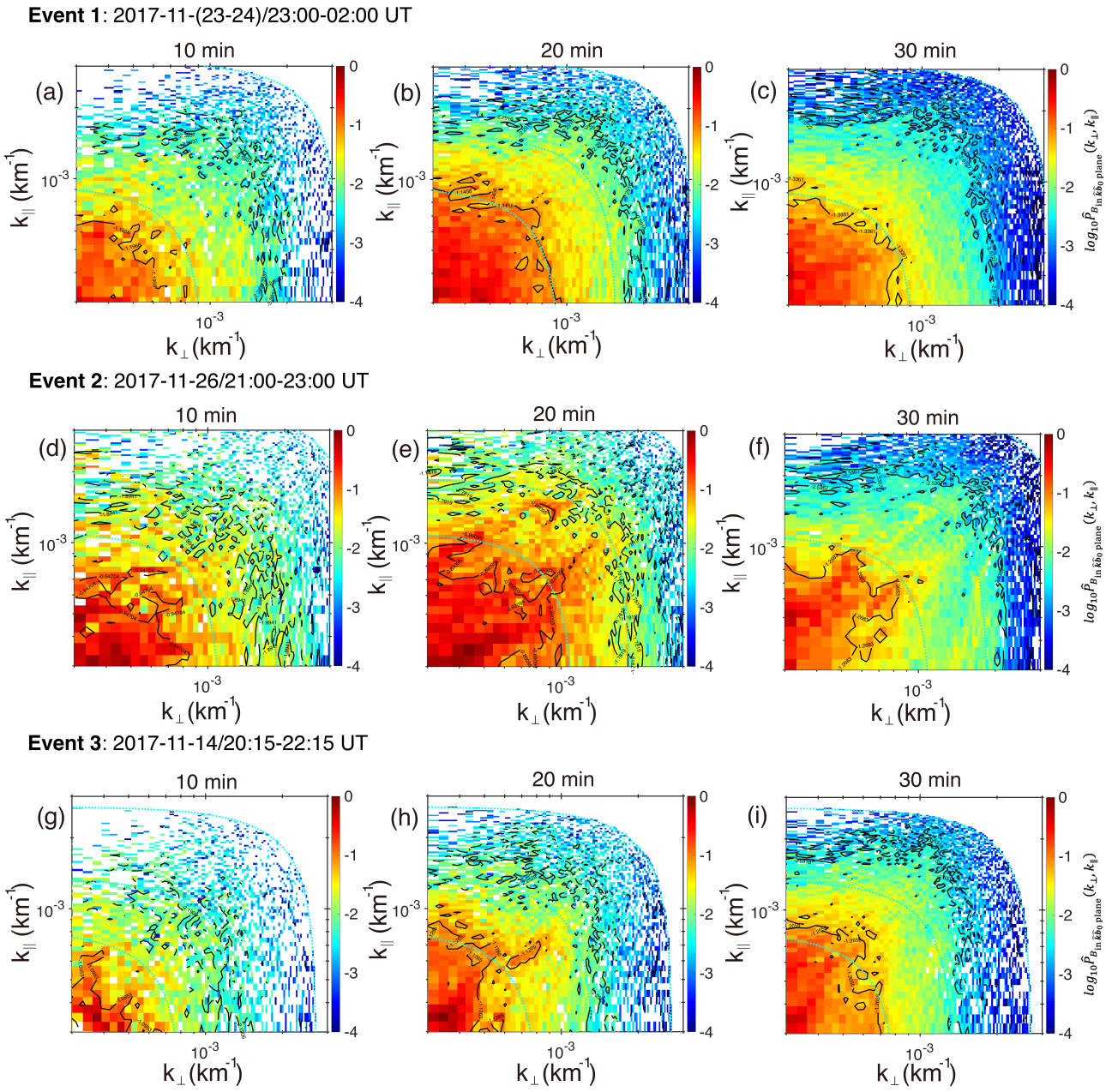

Figure 7. $k_\perp - k_{||}$ wavelet power spectra of magnetic field fluctuations within $\hat{k}\hat{b}_0$ plane using datasets with a length of 10, 20, and 30 minutes, respectively. The magnetic power spectra $\hat{P}_{B_{in\hat{k}\hat{b}plane}}(k_\perp, k_{||}) = (P_{B_{||}}(k_\perp, k_{||}) + P_{B_{\perp 2}}(k_\perp, k_{||}))/(P_{B_{||}} + P_{B_{\perp 2}})_{max}$ are normalized by the maximum power in all bins. (a-c) Event 1: during 23:00-02:00 UT on 2017 November 23-24. (d-f) Event 2: during 21:00-23:00 UT on 2017 November 26. (g-i) Event 3: during 20:15-22:15 UT 2017 November 14. The blue dashed curves represent $k = 0.03/r_{ci}$, $0.05/r_{ci}$, and $0.1/r_{ci}$, respectively.

The primary goal of this study is to investigate the anisotropy and scalings of sub-Alfvénic solar wind turbulence in low-β_p limits at 1 au. We present three representative events of three-dimensional magnetic power spectra in wavevector space using MMS observations. The magnetic power spectra are organized in a new coordinate determined by $\hat{\mathbf{k}}$ and $\hat{\mathbf{b}}_0$ in Fourier space, as described in Section 2.2. This study utilizes two approaches to determine wavevectors: the singular value decomposition method and multi-spacecraft timing analysis. The combination of both methods allows an examination of the properties of magnetic field fluctuations in terms of mode compositions independent of any

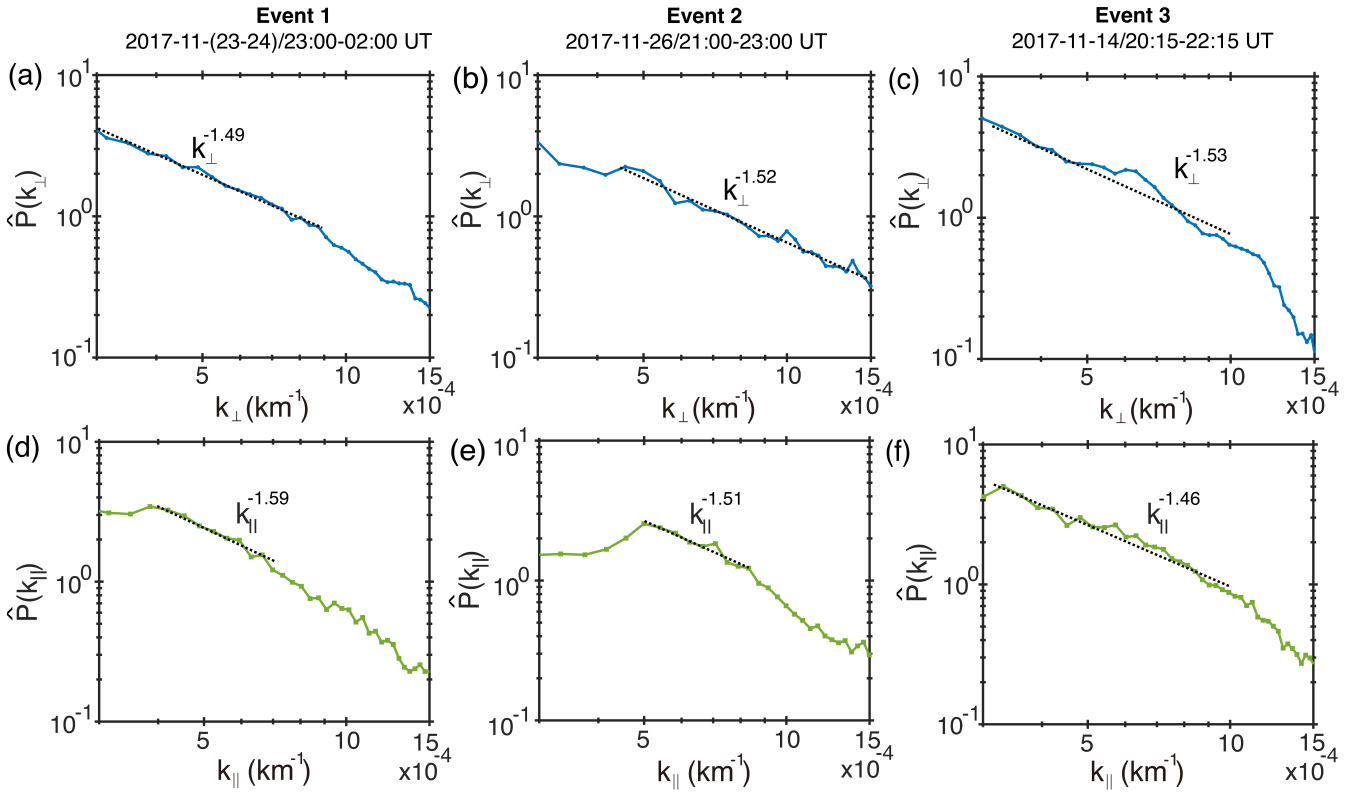

Figure 8. The reduced power spectra of magnetic field fluctuations within $\hat{k}\hat{b}_0$ plane using 30-minute datasets. Blue curve $\hat{P}(k_\perp)$: perpendicular wavenumber spectrum; green curve $\hat{P}(k_{||})$: parallel wavenumber spectrum; black dashed lines: power-law fits. (a,d) Event 1: during 23:00-02:00 UT on 2017 November 23-24. (b,e) Event 2: during 21:00-23:00 UT on 2017 November 26. (c,f) Event 3: during 20:15-22:15 UT 2017 November 14.

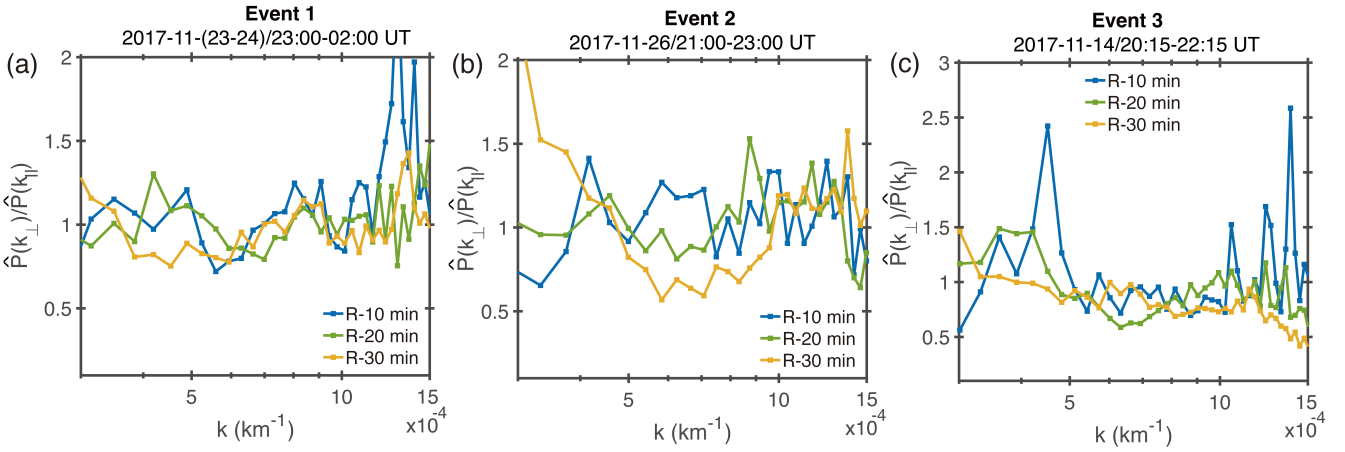

Figure 9. The ratio $\hat{P}(k_\perp)$ to $\hat{P}(k_{||})$ of fluctuations within $\hat{k}\hat{b}_0$ plane. $\hat{P}(k_\perp)$ represents the normalized perpendicular wavenumber spectrum, and $\hat{P}(k_{||})$ represents the normalized parallel wavenumber spectrum. (a) Event 1: during 23:00-02:00 UT on 2017 November 23-24. (b) Event 2: during 21:00-23:00 UT on 2017 November 26. (c) Event 3: during 20:15-22:15 UT 2017 November 14.

spatiotemporal hypothesis. We propose a possible physical explanation of our observations by taking the 30-minute dataset of Event 1 as an example.

4.1. $\delta B_{\perp 1}$ *fluctuations and Alfvén modes*

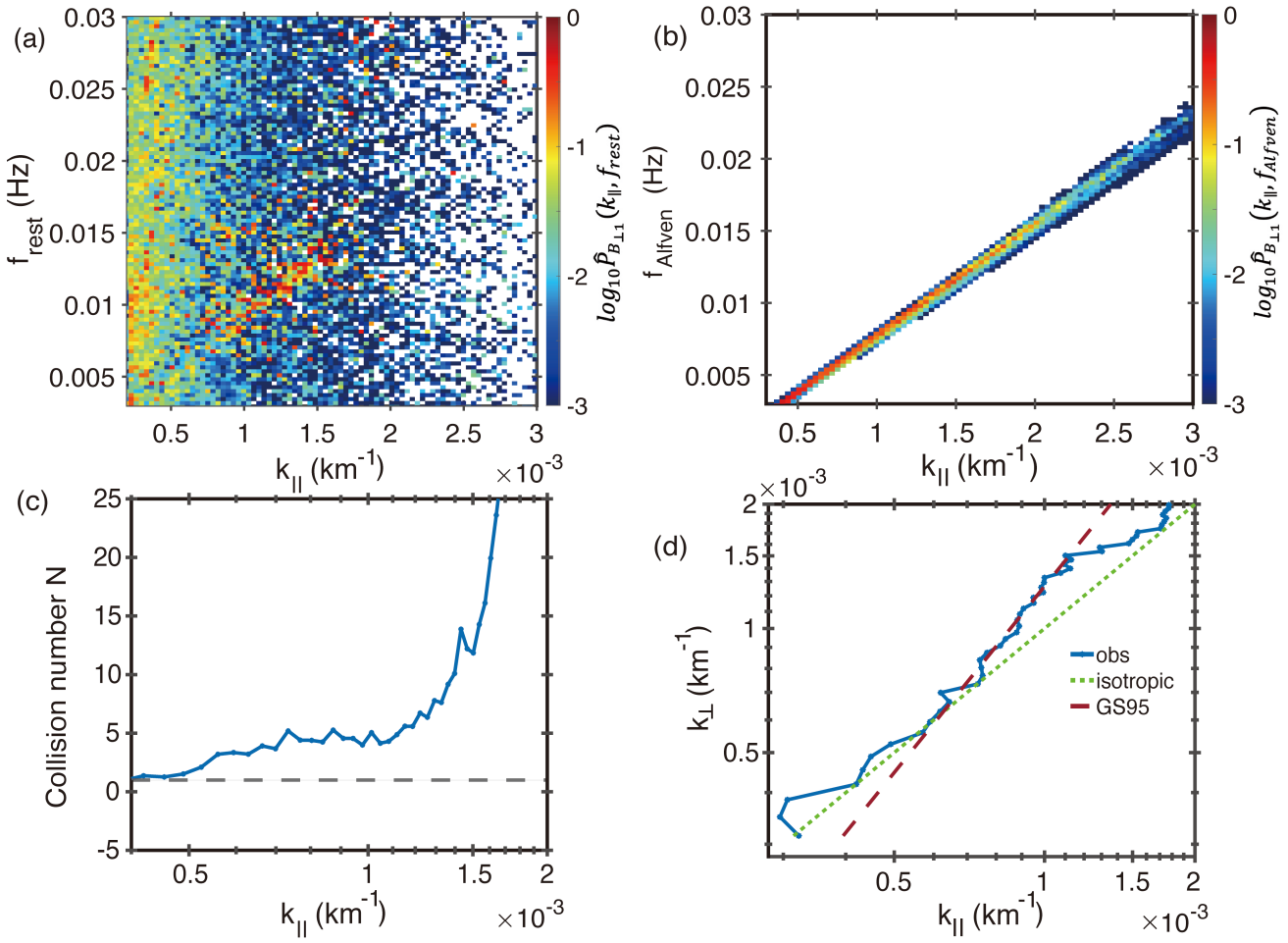

Figure 10. (a) The normalized $f_{rest} - k_{||}$ wavelet power spectra of $\delta B_{\perp 1}$ fluctuations in the rest frame of the solar wind. $\hat{P}_{B_{\perp 1}}(k_{||}, f_{rest}) = P_{B_{\perp 1}}(k_{||}, f_{rest})/P_{B_{\perp 1,max}}(k_{||}, f_{rest})$. (b) The normalized theoretical dispersion relation of Alfvén modes. $\hat{P}_{B_{\perp 1}}(k_{||}, f_{Alfven}) = P_{B_{\perp 1}}(k_{||}, f_{Alfven})/P_{B_{\perp 1,max}}(k_{||}, f_{Alfven})$. (c) Collision number N versus $k_{||}$. The horizontal dashed line marks $N = 1$. (d) The variation of $k_{\perp}$ versus $k_{||}$ for magnetic power of $\delta B_{\perp 1}$ fluctuations (blue curve). The green dashed line represents isotropy $k_{||} = k_{\perp}$. The red dashed line represents the Goldreich-Sridhar scaling $k_{||} \propto k_{\perp}^{\frac{2}{3}}$. These figures use the 30-minute dataset of Event 1.

The frequency f_{rest} is obtained by correcting the Doppler shift $f_{rest} = f_{sc} - \mathbf{k} \cdot \mathbf{V}/2\pi$, where f_{rest} represents the frequency in the rest frame of the solar wind, and f_{sc} represents the frequency in the spacecraft frame. Considering that the SVD method only determines the propagation direction ($\hat{\mathbf{k}}$), we calculate f_{rest} using wavevectors $\mathbf{k}_l$ derived from timing analysis of $\delta B_{\perp 1}$ fluctuations. Thus, $\mathbf{k}_l$ can be expressed as $\mathbf{k}_{\delta B_{\perp 1}}$ here. Although we set a stringent criterion $\phi_{\hat{k}k_l} < 10°$ for $\delta B_{\perp 1}$ fluctuations in section 2.3, $\mathbf{k}_{\delta B_{\perp 1}}$ deviates from the direction of minimum variance vectors of magnetic field fluctuations ($\hat{\mathbf{k}}$), resulting in a f_{rest} uncertainty range between $|f_{sc} - \frac{|k||V_{sw}|cos(\theta_{kV_{sw}} - 10°)}{2\pi}|$ and $|f_{sc} - \frac{|k||V_{sw}|cos(\theta_{kV_{sw}} + 10°)}{2\pi}|$. It is challenging to correct f_{rest} uncertainties because $\phi_{\hat{k}k_l}$ varies with the time t and f_{sc}. To simplify, f_{rest} uncertainties are corrected with uniform angles between $-10°$ and $10°$. The distribution trend will not change when we change the correction angle; thus, our main conclusions are solid.

Figure 10a presents $f_{rest} - k_{||}$ power spectra of $\delta B_{\perp 1}$ in the rest frame of the solar wind after a uniform error correction ($\phi_{\hat{k}k_l} = 10°$). $\hat{P}_{B_{\perp 1}}(k_{||}, f_{rest}) = P_{B_{\perp 1}}(k_{||}, f_{rest})/P_{B_{\perp 1,max}}(k_{||}, f_{rest})$ is normalized by the maximum power in all bins. The magnetic power shows no clear linear relation between the frequency (f_{rest}) and parallel wavenumber ($k_{||}$)

at $k_{||} < 5{\times}10^{-4}\ km^{-1}$. However, a branch of an apparent linear power enhancement exists at $5{\times}10^{-4} < k_{||} < 1.5{\times}10^{-3}$ km^{-1}.

Based on the compressible MHD theory, $\delta B_{\perp 1}$ components of magnetic field fluctuations in the direction perpendicular to $\hat{\mathbf{k}}$ and $\hat{\mathbf{b}}_0$ are expected to consist of Alfvén modes. To further understand magnetic power distributions out of $\hat{k}\hat{b}_0$ plane, we first compare $f_{rest} - k_{||}$ power spectra of $\delta B_{\perp 1}$ fluctuations with Alfvén-mode theoretical dispersion relations. The theoretical frequencies of Alfvén modes are given by

$$\omega_A^2(k_{||}) = k_{||}^2 V_A^2 \tag{4}$$

where V_A is the Alfvén speed. In Figure 10b, we assume that magnetic power is totally provided by Alfvén modes. The theoretical dispersion relation of Alfvén modes is roughly consistent with the apparent linear enhanced branch of magnetic power (Figure 10a). This result provides direct observational evidence that this part of fluctuations may originate from Alfvén modes. It is noteworthy that f_{rest} are slightly higher than theoretical Alfvén frequencies if we do not correct the uncertainty resulting from $\phi_{\hat{k}k_l}$. Comparing observations with the theoretical dispersion relations, we obtain the best match with the error correction $\phi_{\hat{k}k_l} = 10°$.

To further understand the fluctuations without apparent linear relations between the frequency (f_{rest}) and parallel wavenumber ($k_{||}$) at $k_{||} < 5 \times 10^{-4}\ km^{-1}$, we calculate the collision number defined as $N = (\frac{\tau_{nl}}{\tau_A})^2 = (\frac{V_A l_\perp}{v_l l_{||}})^2$, where $\tau_{nl} = \frac{l_\perp}{v_l}$ represents the nonlinear interaction time, $\tau_A = V_A/l_{||}$ represents the linear interaction time, v_l represents perpendicular velocity fluctuations, and $l_\perp(l_{||})$ represents perpendicular (parallel) length scale. The strength of the nonlinear effects can be estimated by the collision number. Therefore, turbulence can be typically divided into weak ($N \gg 1$) and strong ($N >\sim 1$) turbulence regimes. When we analyze magnetic field fluctuations out of $\hat{k}\hat{b}_0$ plane ($\delta B_{\perp 1}$), the collision number can be approximately expressed as $N \sim (\frac{V_A l_\perp}{v_l l_{||}})^2 \sim (\frac{B_0 l_\perp}{\delta B_{\perp 1} l_{||}})^2$. Figure 10c shows collision number N versus $k_{||}$. We summarize the comparisons between $f_{rest} - k_{||}$ spectra and collision numbers as follows: (1) At $k_{||} < 5 \times 10^{-4}\ km^{-1}$, the collision number is very close to 1 (Figure 10c), suggesting strong turbulence. At approximately the same wavenumbers, no clear relation between f_{rest} and $k_{||}$ exists (Figure 10a). It is likely because the fast decay of turbulence within one wave period prevents Alfvén wave to propagate. (2) At $5 \times 10^{-4} < k_{||} < 1.5 \times 10^{-3}$ km^{-1}, the collision number becomes slightly larger than 1 (Figure 10c), suggesting that turbulence becomes relatively weaker. It may be because some physical dissipation mechanisms diminish the turbulent amplitudes, leading to weaker nonlinear dynamics (Howes et al. 2011). Therefore, at approximately the same wavenumbers, apparent linear enhancements of magnetic power are observed in Figure 10a. Noteworthily, we deduce that the turbulence is still in the strong regime because the weak turbulence regime needs more collisions ($N \gg 1$) than what we observed. (3) At $k_{||} > 1.5 \times 10^{-3}\ km^{-1}$, the calculated collision number is of no physical meaning due to the limited data samples (Figure 10a).

In Section 3.1, we have shown that the reduced wavenumber spectra of $\delta B_{\perp 1}$ fluctuations roughly follow the scalings: $\hat{P}(k_\perp) \propto k_\perp^{-\frac{5}{3}}$ and $\hat{P}(k_{||}) \propto k_{||}^{-2}$, consistent with the Goldreich & Sridhar (1995) theory. To obtain a more intuitive wavenumber relationship, we extract the relation of $k_\perp$ versus $k_{||}$ by taking the same values of the magnetic power spectrum at $k_\perp$ and $k_{||}$ axes. Figure 10d shows the variation of $k_\perp$ versus $k_{||}$ for magnetic power of $\delta B_{\perp 1}$ fluctuations (blue curve). The green dashed line represents isotropy $k_{||} = k_\perp$, and the red dashed line denotes the Goldreich-Sridhar scaling $k_{||} \propto k_\perp^{\frac{2}{3}}$. At wavenumber $k_{||} < 1.1 \times 10^{-3}\ km^{-1}$ ($k_\perp < 1.5 \times 10^{-3}\ km^{-1}$), the observed variation of $k_\perp$ and $k_{||}$ follows the Goldreich-Sridhar scaling $k_{||} \propto k_\perp^{\frac{2}{3}}/l_0^{\frac{1}{3}}$, with the normalization consistent with the correlation length l_0 obtained in section 3.1. The collision number N is close to 1 at almost the same parallel wavenumber $k_{||} < 1.1 \times 10^{-3}$ km^{-1} (Figure 10c). Therefore, our observations provide direct evidence for the validity of the Goldreich-Sridhar scaling in the solar wind.

4.2. *Fluctuations within $\hat{k}\hat{b}_0$ plane and magnetosonic modes*

Given that the magnetic power within $\hat{k}\hat{b}_0$ plane only plays a limited role, the reliability of quantitative analysis is questionable. Besides, it is more difficult to uniformly correct f_{rest} uncertainties resulting from $\phi_{\hat{k}k_l}$, because we set a more relaxed criterion $\phi_{\hat{k}k_l} < 30°$ for in-plane fluctuations in order to obtain enough samplings. Therefore, magnetic field fluctuations within $\hat{k}\hat{b}_0$ plane are only discussed qualitatively. Figure 11a shows $f_{rest} - k_{||}$ power spectra of magnetic field fluctuations within $\hat{k}\hat{b}_0$ plane in the rest frame of the solar wind without any angle correction for f_{rest}. $\hat{P}_{in\hat{k}\hat{b}_0 plane}(k_{||}, f_{rest}) = P_{in\hat{k}\hat{b}_0 plane}(k_{||}, f_{rest})/P_{in\hat{k}\hat{b}_0 plane,max}(k_{||}, f_{rest})$ is normalized by the maximum power in

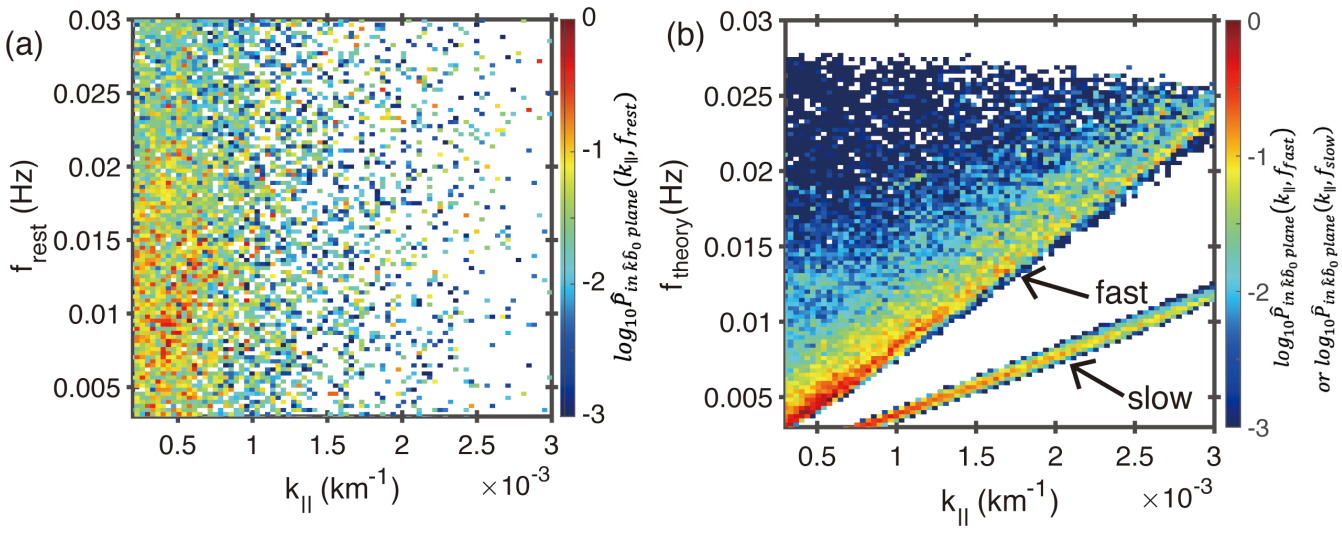

Figure 11. (a) Normalized $f_{rest} - k_{||}$ wavelet power spectra of magnetic field fluctuations within $\hat{k}\hat{b}_0$ plane in the rest frame of the solar wind. $\hat{P}_{in\hat{k}\hat{b}_0 plane}(k_{||}, f_{rest}) = P_{in\hat{k}\hat{b}_0 plane}(k_{||}, f_{rest})/P_{in\hat{k}\hat{b}_0 plane,max}(k_{||}, f_{rest})$ (b) The normalized theoretical dispersion relation of fast and slow modes, where $\hat{P}_{in\hat{k}\hat{b}_0 plane}(k_{||}, f_{fast}) = P_{in\hat{k}\hat{b}_0 plane}(k_{||}, f_{fast})/P_{in\hat{k}\hat{b}_0 plane,max}(k_{||}, f_{fast})$ and $\hat{P}_{in\hat{k}\hat{b}_0 plane}(k_{||}, f_{slow}) = P_{in\hat{k}\hat{b}_0 plane}(k_{||}, f_{slow})/P_{in\hat{k}\hat{b}_0 plane,max}(k_{||}, f_{slow})$. These figures use the 30-minute dataset of Event 1.

all bins. The magnetic power is concentrated in $k_{||} < 1 \times 10^{-3}\ km^{-1}$ and shows no clear relationship between f_{rest} and $k_{||}$.

According to the ideal MHD theory, magnetic field fluctuations within $\hat{k}\hat{b}_0$ plane are most likely provided by compressible magnetosonic modes (fast and slow modes). The theoretical frequencies of fast and slow modes are given by

$$\omega^2_{F,S}(k) = k^2 V_A^2 [\frac{1+\beta_p}{2} \pm \sqrt{\frac{(1+\beta_p)^2}{4} - \beta_p (\frac{k_{||}}{k})^2}] \tag{5}$$

where $k = \sqrt{k_{||}^2 + k_{\perp}^2}$ is the wavenumber, and $k_{||}$ is the parallel wavenumber to B_0. In Figure 11b, we assume that magnetic power spectra are totally provided by fast or slow modes, respectively. Since θ_{kB_0} between $\hat{\mathbf{k}}$ and $\hat{\mathbf{b}}_0$ varies with wavenumbers, fast modes do not show linear dispersion relations (Figure 11b). Given the relatively large uncertainties in f_{rest}, we only focus on the parallel wavenumber distributions of the magnetic power within $\hat{k}\hat{b}_0$ plane. If only fast modes exist, fast-mode magnetic power would roughly cover the wavenumber distributions of the observed magnetic power ($k_{||} < 1 \times 10^{-3}\ km^{-1}$) in Figure 11a. However, if there are only slow modes within $\hat{k}\hat{b}_0$ plane, the magnetic power would be concentrated in larger parallel wavenumbers ($k_{||} > 7 \times 10^{-4}\ km^{-1}$) than actual observations. Overall, it is difficult to identify mode compositions of the fluctuations by comparing the disordered distributions with theoretical dispersion relations.

When assuming the fluctuating velocity $v_{Alfven} \sim v_{slow} \sim v_{fast} \sim V_A$ in low-β_p plasma, the relationship of magnetic fluctuations between fast and slow mode can be expressed as $(\frac{\delta B}{B_0})_{slow} = \sqrt{\beta_p}(\frac{\delta B}{B_0})_{fast}$ (Cho & Lazarian 2003). Therefore, fast modes theoretically provide more magnetic field fluctuations than slow modes in low-β_p plasma (Zhao et al. 2021). For all events studied, the proton plasma β_p is ~ 0.3, in accord with low-β_p limits. Moreover, our observations show that magnetic field fluctuations within $\hat{k}\hat{b}_0$ plane show isotropic behaviors and follow scalings $\hat{P}(k_{\perp}) \propto k_{\perp}^{-\frac{3}{2}}$ and $\hat{P}(k_{||}) \propto k_{||}^{-\frac{3}{2}}$, consistent with the isotropy and scalings of fast modes (Cho & Lazarian 2002; Makwana & Yan 2020). Therefore, indirectly we deduce that magnetic field fluctuations within $\hat{k}\hat{b}_0$ plane more likely originate from fast modes. Quantitative analysis for compressible fluctuations will be the subject of our future studies.

5. SUMMARY

This study presents observations of three-dimensional magnetic power spectra in wavevector space to investigate the anisotropy and scalings of sub-Alfvénic solar wind turbulence in low-β_p plasma at the MHD scale using the MMS spacecraft. The specifics of our findings are summarized below.

1. The magnetic field fluctuations ($\delta B_{\perp 1}$) in the direction perpendicular to $\hat{\mathbf{k}}$ and $\hat{\mathbf{b_0}}$ are prominently stretched perpendicular to $\hat{\mathbf{b_0}}$, indicating a faster cascade in the perpendicular direction. Moreover, such anisotropy increases as the wavenumber increases. The reduced power spectra of $\delta B_{\perp 1}$ fluctuations follow the Goldreich-Sridhar scalings: $\hat{P}(k_\perp) \propto k_\perp^{-\frac{5}{3}}$ and $\hat{P}(k_{||}) \propto k_{||}^{-2}$. $\delta B_{\perp 1}$ fluctuations are more anisotropic using a shorter-interval average magnetic field, suggesting fluctuations are more likely aligned with the local magnetic field than a global magnetic field.

2. The magnetic field fluctuations ($\delta B_{||}$+$\delta B_{\perp 2}$) within $\hat{k}\hat{b}_0$ plane show isotropic behaviors: the perpendicular power distributions are roughly comparable to parallel distributions. The reduced magnetic power spectra within $\hat{k}\hat{b}_0$ plane follow the scalings: $\hat{P}(k_\perp) \propto k_\perp^{-\frac{3}{2}}$ and $\hat{P}(k_{||}) \propto k_{||}^{-\frac{3}{2}}$.

3. Comparing observational frequency-wavevector spectra in the rest frame of the solar wind with theoretical dispersion relations of MHD modes, we find that $\delta B_{\perp 1}$ fluctuations are consistent with Alfvén modes. In contrast, we deduce that the magnetic field fluctuations within $\hat{k}\hat{b}_0$ plane more likely originate from fast modes in low-β_p plasma based on their isotropic behaviors and scalings.

4. We estimated the number (N) of wave packets collisions needed to induce the turbulence cascade. We provide direct observational evidence for the scale-dependent anisotropy from the Goldreich-Sridhar model in the scale range where the critical balance ($N >\sim 1$) holds.

Table 1. Sub-Afvenic fluctuations in low$-\beta_p$ solar wind

time	scale	location	β_p	$< V_{sw} >$	f_{ci}	r_{ci}	$\langle \frac{\delta B}{B_0} \rangle_{30min}$	exponent for $\hat{P}_{\delta B_{\perp 1}}$	exponent for $\hat{P}_{\delta B_{\|}} + \hat{P}_{\delta B_{\perp 2}}$
(UT)	(min)	R_E		(km/s)	(Hz)	km			
(1)	(2)	(3)	(4)	(5)	(6)	(7)	(8)	(9)	(10)
2017-11-(23-24)/23:00-02:00	180	[17,18,6]	0.32	385	0.1	31.8	0.28 ± 0.02	$\hat{P}(k_\perp) \propto k_\perp^{-1.66}, \hat{P}(k_{\|}) \propto k_{\|}^{-2.02}$	$\hat{P}(k_\perp) \propto k_\perp^{-1.49}, \hat{P}(k_{\|}) \propto k_{\|}^{-1.59}$
2017-11-26/21:00-23:00	120	[17,17,6]	0.28	336	0.11	26.7	0.29 ± 0.05	$\hat{P}(k_\perp) \propto k_\perp^{-1.77}, \hat{P}(k_{\|}) \propto k_{\|}^{-2.22}$	$\hat{P}(k_\perp) \propto k_\perp^{-1.52}, \hat{P}(k_{\|}) \propto k_{\|}^{-1.51}$
2017-11-14/20:15-22:15	120	[17,17,6]	0.37	387	0.08	36.9	0.35 ± 0.14	$\hat{P}(k_\perp) \propto k_\perp^{-1.66}, \hat{P}(k_{\|}) \propto k_{\|}^{-2.01}$	$\hat{P}(k_\perp) \propto k_\perp^{-1.53}, \hat{P}(k_{\|}) \propto k_{\|}^{-1.46}$

We would like to thank the members of the MMS spacecraft team, NASA's Coordinated Data Analysis Web, and NASA OMNIWeb. The MMS data and OMNI data are available at https://cdaweb.gsfc.nasa.gov. Data analysis was performed using the IRFU-MATLAB analysis package available at https://github.com/irfu/irfu-matlab and the SPEDAS analysis software available at http://themis.ssl.berkeley.edu.

REFERENCES

Bruno, R., & Carbone, V. 2013, Living Reviews in Solar Physics, 10, doi: 10.12942/lrsp-2013-2

Burch, J. L., Moore, T. E., Torbert, R. B., & Giles, B. L. 2016, Space Science Reviews, 199, 5, doi: 10.1007/s11214-015-0164-9

Cho, J., & Lazarian, A. 2002, Physical Review Letters, 88, 245001, doi: 10.1103/PhysRevLett.88.245001

—. 2003, Monthly Notices of the Royal Astronomical Society, 345, 325, doi: 10.1046/j.1365-8711.2003.06941.x

—. 2009, Astrophysical Journal, 701, 236, doi: 10.1088/0004-637X/701/1/236

Goldreich, P., & Sridhar, S. 1995, The Astrophysical Journal, 438, 763, doi: 10.1086/175121

Grinsted, A., Moore, J. C., & Jevrejeva, S. 2004, Nonlinear Processes in Geophysics, 11, 561, doi: 10.5194/npg-11-561-2004

He, J. S., Marsch, E., Tu, C. Y., et al. 2011, Journal of Geophysical Research: Space Physics, 116, 1, doi: 10.1029/2010JA015974

Horbury, T. S., Wicks, R. T., & Chen, C. H. 2012, Space Science Reviews, 172, 325, doi: 10.1007/s11214-011-9821-9

Howes, G. G., Tenbarge, J. M., & Dorland, W. 2011, Physics of Plasmas, 18, doi: 10.1063/1.3646400

Kraichnan, R. H. 1965, Physics of Fluids, 8, 1385, doi: 10.1063/1.1761412

Makwana, K. D., & Yan, H. 2020, Physical Review X, 10, 031021, doi: 10.1103/PhysRevX.10.031021

Matthaeus, W. H., & Goldstein, M. L. 1982, Journal of Geophysical Research, 87, 6011, doi: 10.1029/JA087iA08p06011

Matthaeus, W. H., Goldstein, M. L., & Roberts, D. A. 1990, Journal of Geophysical Research, 95, 20673, doi: 10.1029/JA095iA12p20673

Narita, Y., Sahraoui, F., Goldstein, M. L., & Glassmeier, K.-H. 2010, Journal of Geophysical Research: Space Physics, 115, n/a, doi: 10.1029/2009JA014742

Oughton, S., Matthaeus, W. H., Wan, M., & Osman, K. T. 2015, Philosophical Transactions of the Royal Society A: Mathematical, Physical and Engineering Sciences, 373, 20140152, doi: 10.1098/rsta.2014.0152

Peredo, M., Slavin, J. A., Mazur, E., & Curtis, S. A. 1995, Journal of Geophysical Research, 100, 7907, doi: 10.1029/94JA02545

Pollock, C., Moore, T., Jacques, A., et al. 2016, Space Science Reviews, 199, 331, doi: 10.1007/s11214-016-0245-4

Roberts, O. W., Nakamura, R., Torkar, K., et al. 2020, The Astrophysical Journal Supplement Series, 250, 35, doi: 10.3847/1538-4365/abb45d

Roelof, E. C., & Sibeck, D. G. 1993, Journal of Geophysical Research, 98, doi: 10.1029/93ja02362

Russell, C. T., Anderson, B. J., Baumjohann, W., et al. 2016, Space Science Reviews, 199, 189, doi: 10.1007/s11214-014-0057-3

Santolík, O., Parrot, M., & Lefeuvre, F. 2003, Radio Science, 38, doi: 10.1029/2000RS002523

Shebalin, J. V., & Montgomery, D. 1983, Journal of Plasma Physics, 29, 525, doi: 10.1017/S0022377800000933

Taylor, G. I. 1938, Proceedings of the Royal Society A: Mathematical, Physical and Engineering Sciences, 164, 476, doi: 10.1098/rspa.1938.0032

Tu, C. Y., & Marsch, E. 1995, Space Science Reviews, 73, 1, doi: 10.1007/BF00748891

Verscharen, D., Klein, K. G., & Maruca, B. A. 2019, Living Reviews in Solar Physics, 16, 5, doi: 10.1007/s41116-019-0021-0

Yan, H., & Lazarian, A. 2002, Physical Review Letters, 89, 281102, doi: 10.1103/PhysRevLett.89.281102

—. 2004, The Astrophysical Journal, 614, 757, doi: 10.1086/423733

—. 2008, The Astrophysical Journal, 673, 942, doi: 10.1086/524771

Zhao, S. Q., Yan, H., Liu, T. Z., Liu, M., & Shi, M. 2021, The Astrophysical Journal, 923, 253, doi: 10.3847/1538-4357/ac2ffe